International Journal of Innovative Research in Computer Science & Technology (IJIRCST)
ISSN: 2347-5552, Volume-10, Issue-1, January 2022
https://doi.org/10.55524/ijircst.2022.10.1.11
Article ID IJIRD-1158, Pages 66-72
www.ijircst.org

Improve the Photovoltaic Performing of Carbon-Form Perovskite Solar Cells

Deepak Choudhary

Department of Physics, D.J. College, Baraut, Uttar Pradesh, India

Correspondence should be addressed to Deepak Choudhary; choudharydeepak962@gmail.com

ABSTRACT- A solvent-assisted approach was established to make CH3NH3PbI3 perovskite absorber layers. A mixture of CH3NH3I, PbI2, c-butyrolactone, and dimethyl sulfoxide (DMSO) was used, followed by the addition of chlorobenzene (CB). The approach produced ultra-flat and dense perovskite capping layers atop mesoporous films TiO2, allowing for a significant boost in the performance of carbon electrode-form perovskite solar cells using free whole transport material (HTM) (PSCs). As a comparative solvent, toluene (TO) was also investigated. The generated HTM-free PSCs form on drop-casting CB showed a power conversion efficiency (PCE) of 9.73 percent at an annealing temperature of 100 C, which is 36 and 71 percent greater than those fabricated from perovskite films using TO or without adding an additional solvent, respectively. The interaction between the intermediate phase of PbI2–DMSO–CH3NH3I and the extra solvent was discussed. The effect of annealing temperature on absorber film development, morphology, and crystalline structure was also examined, and the results were connected with photovoltaic performance. Highly efficient, simple, and stable HTM-free solar cells with a PCE of 11.44 percent were created using the best perovskite absorbers annealed at 120 C.

Keywords- Perovskite, Solar Cells, Carbon Form, Photovoltaic, Spin coating

I. INTRODUCTION

Over the last five years, there has been a surge in interest in the study of organic–inorganic hybrid perovskite compounds for applications in photovoltaic devices due to their low cost, simple fabrication technique, and high efficiency solar power conversion. Perovskite solar cells (PSCs) typically consist of a mesoporous titania or alumina scaffold, a methylammonium (MA) lead iodide perovskite light absorber, an organic hole transport material (HTM), typically spiro-OMeTAD (2,20,7,70-tetrakis-(N,N-di-p-methoxyphenylamine)-9,90 In 2012, PSCs attained a power conversion efficiency (PCE) of 10%. Because of its good optical transparency and flawless band alignment with respect to CH3NH3PbI3, TiO2/spiro-OMeTAD is considered a successful couple. Later, utilising a two-step sequential deposition process, including of a PbI2 spin-coating followed by exposure to a CH3NH3I solution to generate CH3NH3PbI3, or a dual-source vapour deposition technique to manufacture a planar heterojunction solar cell, the PCEs were improved by 15%. Then, an yttrium-doped TiO2 layer, a mixed halide perovskite CH3-NH3PbI3-xClx absorber, employing a polyethyleneimine ethoxylated modified ITO electrode, and spiro-OMeTAD, a planar structured PSC with a PCE of 19.3 percent was developed. Triple Cs/MA/for-mamidinium cation PSCs have recently achieved a power output of 21.1 percent.

The majority of research PSC devices currently use gold as the back contact, with organic whole conductors acting as electron-blocking or hole transport layers. The exorbitant cost of pure whole transportation materials makes these cells prohibitively expensive. Furthermore, hole conductors like the commonly used spiro-OMeTAD are not only expensive, but they can also cause moisture-induced degradation in PSCs, particularly when coupled with hygroscopic dopants like lithium bis (trifluoromethanesulfonyl) imide. Etgar et al. hypothesised and published HTM-free perovskite photovoltaics to overcome the lifetime-limiting difficulties with organic whole transporters. With gold as a back electrode, HTM-free PSCs obtained efficiencies of around 10%. The valuable Au electrode also necessitates a high-vacuum, high-cost evaporation process, which limits its future use. The best PSCs are now competitive with current commercial technology in terms of efficiency, and they are potentially considerably cheaper. Commercial solar cells, on the other hand, must survive 20–30 years with negligible degradation. Long-term stability in a variety of situations is the most difficult challenge facing PSCs.

Because its function is comparable to that of Au, low-cost nano-carbon could be a good material to replace Au as a back contact in PSCs. Carbon nanomaterials have been shown to be excellent counter-electrode candidates for use in dye-sensitized solar cells (DSSCs) over the last decade, owing to a variety of intriguing properties such as high electrical conductivity, thermal stability, good optical transparency, unique nanostructure, excellent electrocatalytic activity, low cost, and abundance. Carbon nanomaterials have made significant progress in DSSCs. Nevertheless, perovskite organic lead iodide is unstable at

high temperatures or in some solvents. As a result, there are some issues with preparing a carbon layer directly. In the beginning, or CH3NH3PbI3, mixed-cation 5-ammoniumvaleric (5-AVA) and MA perovskite (5-AVA) x (MA) x (PbI3) were infiltrated into a high-temperature prefabricated monolithic device composed of four layers: ZrO2 mesoporous, TiO2 mesoporous, TiO2 dense, and z

In this paper, we describe a solvent-assisted chlorobenzene (CB)-form technique for making simple, stable, and efficient HTM-free PSCs with carbon counter electrodes, mixed solution a spin-coating of CH3NH3I, GBL, PbI2, and DMSO, followed by DC TO or CB during spinning, resulted in CH3NH3PbI3 absorber layers on mesoporous TiO2 films. For comparison, TO was investigated as a DC solvent. The influence of the DC solvent and annealing temperature on thin film shape, crystal structure, and solar cell efficiency was studied. Extremely homogeneous dense and perovskite layers capping above mesoporous TiO2 films were produced by altering the DC solvent and tweaking the annealing temperature, allowing the construction of significantly better HTM-free PSCs. Simple, structured, HTM-free solar cells have a high efficiency of 11.42 percent. The carbon-form PSC devices thus obtained have shown substantially better stability than the HTM devices.

II. EXPERIMENTAL

A. Resources

All materials were acquired from Alfa Aesar or Sigma-Aldrich and utilised as received, unless otherwise noted. Merck KGaA and Lumi-nescence Technology Corp. sold Spiro-MeOTAD to each other. In a recent study, MA iodide (MAI) CH3NH3I was produced.

B. Device Production

Etching with Zn powder and 2 M HCl patterned fluorine-doped tin oxide-coated glass (Pilkington TEC 15). After cleaning with surfactant, the etched substrate was rinsed with acetone, ethanol, and deionized water. A technique described in our previous work was used to synthesise a 50-nm dense TiO2 compact (c-TiO2) thin film. The porous TiO2 (p-TiO2) layer was created by spin-coating TiO2 commercial paste (Dyesol 18NR-T) dissolved in ethanol (1:2.5 weight ratio) at 5000 rpm for 30 seconds and then heating at 500 LC for 30 minutes. After cooling to room temperature, the as-prepared nanoporous TiO2 layers were dipped in aqueous solution 40 mM TiCl4 for 30 minutes at 70 LC, dried at ambient atmosphere, and sintered at 500 LC for 30 minutes.

The solvent engineering method reported by Jeon et al. was modified to create CH3NH3PbI3 perovskite absorber layers. This was done in a glove box with a 10% relative humidity. The powders of CH3NH3I (0.1975 g) and PbI2 lead iodide (0.5785 g) were agitated at 60 LC for 12 hours in a combination of GBL (700 lL) and DMSO (300 lL). A successful two-step spin-coating method at 2000 rpm for 50 s and 3500 rpm for 50 s was used to deposit the generated precursor solution onto the c-TiO2/ FTO/p-TiO2 substrate. The second stage involved dripping anhydrous CB or TO into the middle of the sample 30 seconds before the procedure ended. On a hot plate, the perovskite precursor-coated substrate was heated and dried for 10 minutes at 50–140 LC.

The carbon electrodes were made by doctor blade coating the growing perovskite absorber with LT conductive carbon ink then drying at 100 LC for 30 minutes. For comparison, Spiro-OMeTAD was placed onto the perovskite absorber for comparison, and the metal cathode was coated on the spiro-OMeTAD HTM layer by thermal evaporation under a base pressure of 6–9.

C. Identification

Expending a field emission scanning electron microscope, the morphologies of perovskite absorbers were studied at various post-heating temperatures and with various DC solvents (FESEM, Hitachi S4800). Expending an diffractometer X-ray (Bruker D8 Davinci instrument, Cu Ka: k = 0.15406 nm), the structures of the produced perovskite absorbers were discovered. Measurements of photocurrent density–voltage (J–V) were carried out using an AM 1.5 solar simulator with a 1000 W xenon lamp (Model No. 91192, Oriel, USA). A typical silicon cell was used to calibrate the solar simulator (Newport, USA). On the test cell's surface, the light intensity was 100 mW/cm-2. In the reverse direction, J–V curves were measured using a computer-controlled digital source metre (Keithley 2440). A metal aperture mask with an opening of roughly 0.09 cm2 was utilised to characterise the device's photovoltaic performance.

III. DISCUSSION

Using the solvent engineering method, we first studied the consequence of solvent DC on the morphology of CH3NH3PbI3 perovskite films produced on p-TiO2. The CH3NH3PbI3 absorber's post-heating temperature is 100 LC. Figure 1 shows optical and SEM images of layers CH3NH3PbI3 produced with or without a DC solvent (CB or TO). Non-homogeneous perovskite film was generated in the sample without DC solvent, and very large branch-like grains with a significant portion of the substrate (the p-TiO2 layer) exposed without CH3NH3PbI3 coverage are seen in Figure-1a, b, which is consistent with earlier observations. As shown in the inset of Figure-1b, a higher magnification SEM image of these huge branch-like grains indicates that the grain structure is made up of crystals with diameters ranging from 50 to 400 nm. When the semiconductor perovskite CH3NH3PbI3 was deposited by a single-step spin-coating from a solution of PbI2 and CH3NH3I and in GBL or N, N-dimethylformamide (DMF), crystals with a wide range of sizes were also found. When TO was used as a DC solvent, the huge branch-like grains in the optical picture in Fig. 1c vanished, and some smaller (35–140 nm) and more uniform crystals began to form, resulting in lower pinhole sizes and improved perovskite surface coverage, as shown in Figure-1d. When CB was utilised as a DC solvent, on the other hand, the mesoporous TiO2 layer was completely covered with interconnected crystals, as shown in the inset of Figure-1f. The

CH3NH3PbI3 films produced by adding CB are made up of sub-micron particles.

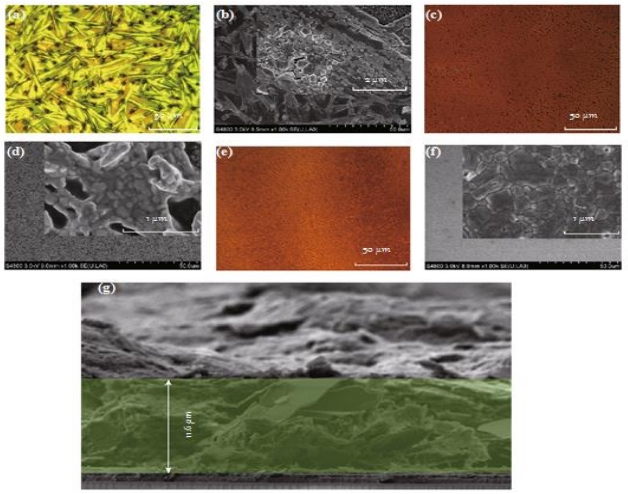

Figure 1: SEM images and Optical of layers CH3NH3PbI3 manufactured with toluene (c, d) or chlorobenzene (e, f) as a drop-casting solvent (a, b). (g) photo of the PSCs in cross-section by FESEM

(100–550 nm)-sized grains, which are clearly larger than those seen in the absorber layer when TO is used as a DC solvent. The top surface of the former has a dense-grained morphology. Differences in perovskite film surface coverage on the p-TiO2 layer are anticipated to alter device properties. Figure 1g shows a cross-section FESEM picture of the PSCs. In comparison to the other functional layers in the device, the produced carbon film is quite thick. The carbon layer is approximately 11.6 lm thick. It has a sheet resistance of approximately 14.6 X sq-1. The carbon sheet adhered well to the underlayer of CH3NH3PbI3 and completely covered the absorber.

Figure 2 depicts the XRD patterns of the three samples mentioned above. The red, blue, and purple curves represent XRD spectra obtained after layers CH3NH3PbI3 without solvent DC, CB, and TO, respectively. Diffraction peaks detected at 14.02L, 28.32L, 31.76L, 40.46L, and 43.02L correspond to reflections from the tetragonal perovskite structure's (110), (220), (310), (224), and (314) crystal planes, respectively. When compared to the case of the pristine absorber, it was discovered that

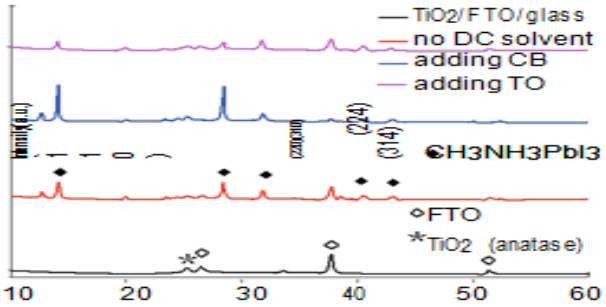

Figure 2: Spectra XRD of layers CH3NH3PbI3 produced without or using chlorobenzene (CB) or toluene (TO) as a drop-casting (DC) solvent

With the addition of CB, intense diffraction peaks on both the (110) and (220) faces became greatly enhanced, indicating that the CH3NH3-PbI3 film's crystalline quality improved dramatically. In addition, as the morphology evolves from branch to plate, the optical and SEM pictures show larger crystalline domains in the lateral direction Figure-1. However, when TO was added to the mixture, both the (110) and (220) peaks were noticeably lower, which can be attributed to the lower quality of the perovskite crystals in the latter, as shown in the inset of Fig. 1b, d.

Carbon electrode-form PSCs were produced without a DC solvent or with CB or TO as a DC solvent to see how the additional solvent affected the HTM-free device performance. The $CH_3NH_3PbI_3$ absorber's post-heating temperature is 100 LC. 8–12 PSCs were manufactured in the same manner for each device fabrication condition.

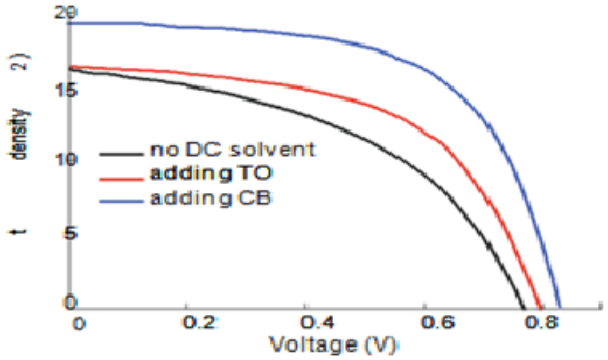

Figure 3: For J–V curves for CH3NH3PbI3 layers manufactured without a drop-casting (DC) solvent or using chlorobenzene (CB) or toluene (TO) as a DC solvent for carbon-form solar cells

Table 1 lists the photovoltaic parameters that equate to short circuit current density (JSC), circuit open fill factor (FF), voltage (VOC), and PCE. The PSC with the immaculate perovskite film had a JSC of 16.10 mA cm-2, a and an FF of 0.46, resulting in an overall PCE of 5.70 percent, VOC of 0.77 V, as shown in Fig. 3 and Table 1. The constructed device had an improved an FF of 0.55, VOC of 0.80 V, and a similar JSC of 16.31 mA cm-2 when using TO droplets, resulting in a PCE improvement of 7.17 percent, resulting in a PCE improvement of nearly 26 percent. Surprisingly, after CB was introduced perovskite precursor layer, the PCE increased by 9.73%.The addition of CB droplets improved all device characteristics at the same time, such as increasing JSC from 16.10 to 19.21 mA cm-2, VOC from 0.77 to 0.83 V, and FF from 0.46 to 0.61, resulting in a 71 percent increase in PCE in the device.

The development of the CH3NH3I–PbI2–DMSO intermediate phase during spin-coating from MAI, DMSO, and PbI2 could explain the shape and crystal structure evolution of the perovskite film with CB droplet treatment exhibited in Figs. 1 and 2. In the same way as a TO DC transforms MAI-PbI2–DMSO into MAPbI3, this process transforms MAI-DMSO-PbI2 into MAPbI3. Jeon et al. used a mixture of DMSO/GBL and a TO drip to deposit superior

(I1-xBrx) 3 (x = 0.1–0.15) CH3NH3Pb perovskite layers. They discovered that the PbI2–DMSO–MAI spin-coated phase intermediate had an extraordinarily uniform and flat morphology, that the intermediate phase was partially changed into perovskite phases at 100 LC, and that the complete transformation into CH3NH3Pb (I1-xBrx)3 occurred at 130 LC. As shown in Figure-2, pure perovskite phases were produced at 100 LC for treatment with both CB and TO in our synthesis. Our findings are consistent with those reported in. With the help of CB, high-quality CH3NH3PbI3 films were created for a rapid deposition–crystallisation method at 100 LC.

In solution processes, thermal energy directly dominates the thermodynamics of crystalline perovskite film production. Controlling the perovskite precursor film's thermal annealing process is crucial for optimal performance [17, 34]. In this study, we discovered that the annealing temperature has a significant impact on the quality of the perovskite absorber. Figure 4 shows the XRD patterns of perovskite films produced on p-TiO2 at varied annealing temperatures using a solvent-assisted technique. A CB treatment was used to create the CH3NH3PbI3 layers. The temperature of the post-heating was increased from 50 to 140 LC. When a low annealing temperature of 50 LC is used, XRD peaks at the low angles of 7.21L and 9.17L can be seen.

Table 1: shows the photovoltaic presentation of solar cells with layers CH3NH3PbI3 produced with or without an aided solvent (chlorobenzene or toluene)

Samples	JSC (mA cm-2)	FF	VOC (V)	PCE (%)	RS (X cm2)	RSH (X cm2)
No drop-casting solvent	16.10	0.46	0.77	5.70	129	1996
Adding chlorobenzene	19.21	0.61	0.83	9.73	73	11,175
Adding toluene	16.31	0.55	0.80	7.17	121	4601

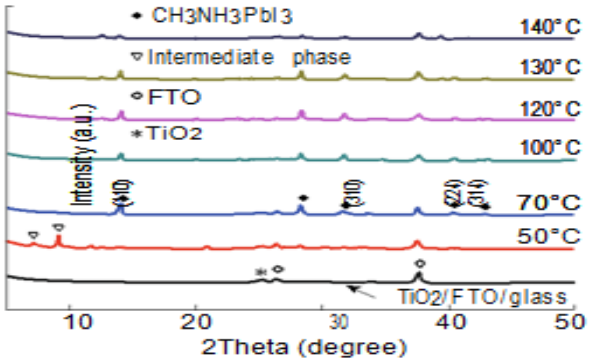

Figure 4: Patterns of Perovskite XRD films produced on p-TiO2 using chlorobenzene drop-casting at temperatures ranging from 50 to 140 LC

This may be attributable to the film's intermediary phase of MAI–PbI2–DMSO. Only a minor peak at 9.17L was noticed when the annealing temperature was increased to 70 LC. XRD peaks at low angles vanished completely when the annealing temperature was equal to or greater than 100 LC. Peaks at 14.02L, 28.32L, 31.76L, 40.46L, and 43.02L, corresponding to reflections from the (110), (220), (310), (224), and (314) crystal planes of the tetragonal perovskite structure, respectively, were found when the annealing temperature was equal to or greater than 70 LC. For our pure halide material system with CB DC, the XRD data showed that the MAI -PbI2- -DMSO phase intermediate was totally converted into perovskite phases at 100 LC. In addition, the XRD pattern for the absorber generated at 120–140 LC shows a tiny peak at 12.66L, which is related to the PbI2 film. The intensity of this PbI2 phase peak grew as the temperature increased from 120 to 140 LC, while the intensity of the perovskite phase peaks declined. It's worth noting that annealing at 120 LC resulted in the majority of the precursor film being converted to the active perovskite phase, with only a small portion of PbI2 remaining, as evidenced by the minor peak at 12.66L. Despite the fact that this peak represents conversion incomplete of the MAI-PbI2–DMSO–film to the active perovskite phase, the presence of a small amount of residual PbI2 has been observed to improve most device performance likely due to passivation of surface and grain boundary states.

Figure 5 shows optical and SEM pictures of perovskite films produced on p-TiO2 using the solvent-assisted technique at 120–140 LC and CB DC annealing temperatures. The development of a plate-like, homogenous, and well-crystallized perovskite layer was achieved by annealing at 120 LC. The entire layer atop the p-TiO2 seen in the inset of Fig. 5b is composed of homogeneous, interconnected, and precisely formed crystals with 100% surface coverage. The ideal absorber layer is made up of sub-micron (250–750 nm) sized grains that are other identical and those larger than in the film CH3NH3PbI3 generated with CB treatment and a 100 LC annealing temperature (Fig. 1e, f). However, as the annealing temperature rose above 120 LC, the quality of the resulting absorber deteriorated, and the perovskite's surface coverage dropped. The developed absorber layer is made up of sub-micron-sized grains at 130 LC, with some of the p-TiO2 layer exposed without CH3NH3PbI3 covering, as shown in the inset of Figure- 5d. As shown in the inset of Figure-5f, annealing at 140 LC resulted in bigger pinhole sizes and poorer surface coverage of perovskites.

PSCs were built using CH3NH3PbI3 absorbers produced via DC CB and annealed at varied temperatures from 100 to 140 LC to evaluate the effect of annealing temperature on HTM-free device performance. At each temperature, 8–12

PSCs were produced in the same way. Figure 6 shows the average device characteristics, with the related photovoltaic parameters reported in Table-2. The annealing temperature of per-ovskite and the device's photovoltaic performance were shown to be inextricably linked. As a result of the JSC, VOC, and FF, samples produced at 120 LC had the greatest PCE, 11.44 percent. 0.60 V, 21.43 mA cm-2, and 21.43 mA cm-2, in that order. As a result of the JSC, VOC, and FF, devices developed at 130 LC had a very high PCE of 10.21 percent. 0.84 V, 19.29 mA cm-2, and 0.63, in that order. However, as the annealing temperature was raised above 130 LC, the annealing process became more difficult.

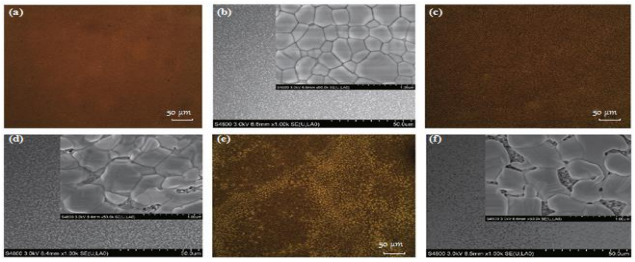

Figure 5: Optical and SEM photos of perovskite films formed on p-TiO2 using chlorobenzene drop-casting at various annealing temperatures: a, b 120 LC, c, d 130 LC, and e, f 140 LC

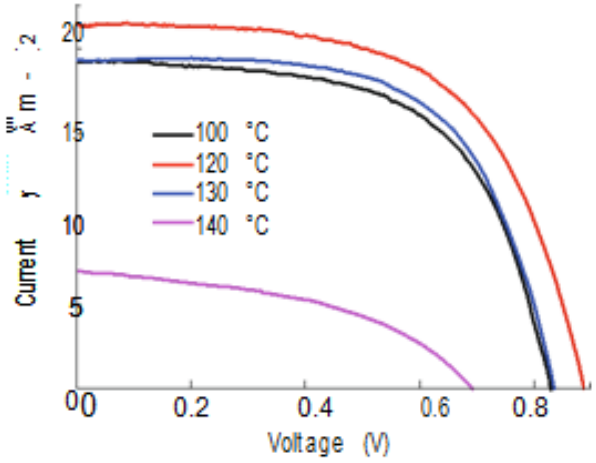

Figure 6: show in J–V curves for solar cells with layers CH3NH3PbI3 produced by chlorobenzene drop-casting at 120–140 LC annealing temperatures

The JSC, VOC, and FF values all dropped significantly, resulting in a significant drop in PCE. The device with 120 LC has the best photovoltaic performance due to the highest crystalline, morphological, and surface coverage quality of its absorber, as illustrated in Figure 4 and 5. The results described in are compatible with these experimental findings. The IPCE spectra of these four devices for monochromatic incident photon-to-electron conversion efficiency (IPCE) are given in Fig. 7. Apart from the PSCs with a 140 LC annealing temperature, the other three showed broad and effective photoelectric conversion across the visible light spectrum. Over the entire spectral range between 300 and 800 nm, the devices with 120 and 130 LC achieved substantially greater IPCEs than the cells with 140 LC, mirroring the difference in photocurrents observed for these devices shown in Fig. 6 and Table 2.

The series resistance (RS) and shunt resistance (RSH) were also calculated using the J–V characteristics given in Figures 3 and 6. Tables 1 and 2 present a summary of the RS and RSH data. In solar cells, keeping the RS as low as possible is critical because a high RS will reduce JSC, VOC, and FF, and hence PCEs. The RS after the addition PSC with the of CB is 73 X cm2 for devices with 100 LC, is lesser than 121 or 129 X cm2 for devices with TO or without DC solvent, respectively. When the temperature of the CB treatment was increased from 100 to 130 LC, the RS remained at modest levels of about 70 X cm2. However, when the temperature was raised to 140 LC, the device's RS climbed to 293 X cm2. The low RS of the device with CB and annealing temperatures of 100–130 LC is owing to the high-quality perovskite layer's modest contact resistance and low bulk resistance, indicating that high cur at low applied voltages, rents can flow through the cell. Shunt resistance (RSH) is usually caused by a junction p–n.

Table 2: Photovoltaic performance of solar cells with layers CH3NH3PbI3 produced with chlorobenzene help at 120–140 LC annealing temperatures

Annealing T (LC)	JSC (mA cm-2)	FF (%)	VOC (V)	PCE (%)	RS (X cm2)	RSH (X cm2)
100	19.21	0.61	0.83	9.73	73	11,175
120	21.43	0.60	0.89	11.44	74	18,808
130	19.29	0.63	0.84	10.21	70	22,404
140	6.93	0.45	0.69	2.15	293	3495

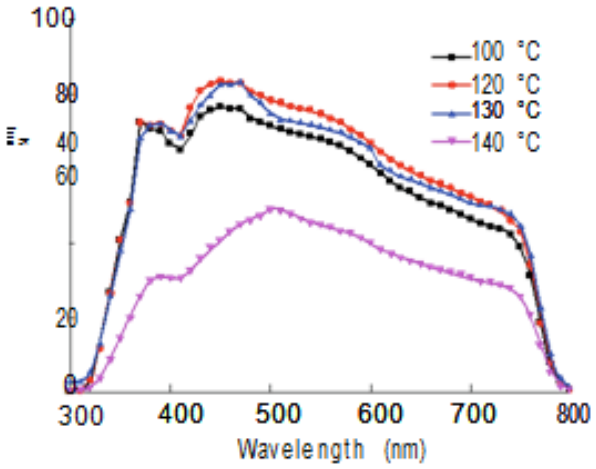

Figure 7: Spectra IPCE of solar cells with layers CH3NH3PbI3 manufactured by chlorobenzene drop-casting at 120–140 LC annealing temperatures

Towards the junction, non-idealities and impurities cause partial junction shortening, especially near cell margins. To avoid current loss at the junction, the RSH must be greater, lowering the photocurrent and, as a result, the solar cell performance. The pinholes generated in result managed CH3-NH3PbI3-xClx absorbers have been widely documented to cause direct contact between the p-type spiro-OMeTAD and the compact layer TiO2, resulting in a shunting route that is likely partially responsible for the low FF and open circuit voltage in devices. The holes or vacancies layer capping on the layer p-TiO2 resulting in the lowest FF and VOC in the device with a pristine absorber, and induced the second least RSH, caused the least RSH, resulting in the second lowest FF and VOC in the device via dropwise TO application, as indicated in Table 1. The smoother perovskite layer created by injecting TO or CB into the spin-coated perovskite precursor layer made after a mixed result of PbI2, CH3NH3I, DMSO, and GBL reduced the cell's series resistance and raised the shunt resistance, resulting in better photovoltaic effects Table 1. When the temperature was increased from 100 to 130 LC with the CB treatment, the shunt RSH grew in resistive value, but when the temperature was increased to 140 LC, the pinholes or voids in the layer capping on the p-TiO2 layer generated resulting in the lowest FF, the least RSH. Traditional solvents for developing perovskite absorbers have quite high boiling points, with values of 153 and 204–205 LC for N, N-dimethyl-methanamide (DMF) and GBL, respectively. Due to the comparatively long drying durations of solution-coated films, such high boiling temperatures might result in large-area thickness fluctuations or dewetting/ shrinkage of the casting precursor solution. The proposed solvent-assisted method in our study comprised mixed result spin-coating of CH3NH3I, GBL/DMSO, and PbI2, then spinning DC CB or TO. At room temperature, TO boiling point 111 LC, vapour pressure 22 mmHg and CB boiling point 132 LC, vapour pressure 11.8 mmHg have a significantly lower boiling point and a significantly higher vapour pressure than DMSO (boiling point 189 LC, vapour pressure 0.6 mmHg) and GBL boiling point 204–205 LC, vapour pressure 1.5 mmHg Considering the physical properties of the solvents, at the beginning of the spin-coating process, the precursor film was composed of PbI2 and MAI dissolved in the DMSO/GBL solvent mixture, and the precursor film continued to thin because liquid flowed radially owing to the action of centrifugal force, and sol-vent evaporation was ignored, whereas in the intermediate stage, the composition of the film was concentrated by the evaporation of GBL due to its higher vapour. Then, during the second spinning stage, the addition of TO or CB droplets with a very high vapour pressure caused instantaneous freezing of the constituents on spinning and the rapid creation of the MAI–PbI2–DMSO phase, resulting in a full and even precursor layer. DMSO was used to assist in slowing down the fast interaction among the inorganic CH3NH3I and PbI2 components of perovskite during the spin-coating process.

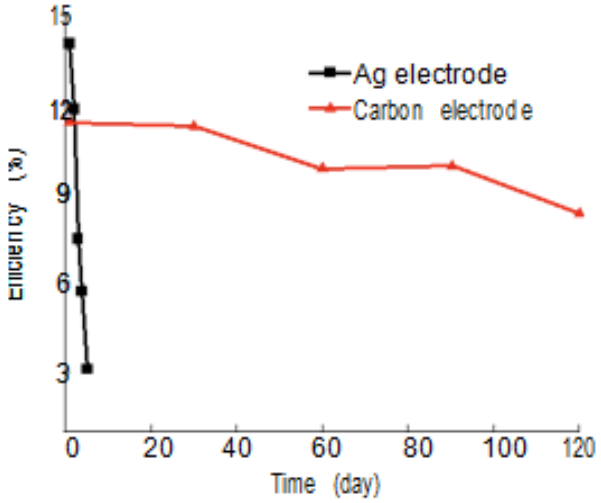

Figure 8: Stability profiles of non-sealed c-TiO2/FTO/CH3NH3PbI3/p-TiO2/spiro-MeOTAD/Ag (squares) and c-TiO2/FTO/CH3NH3PbI3/p-TiO2 carbon (triangles) perovskite solar cells. The gadgets were housed in a dry electronics cabinet with no nitrogen (10 percent RH, room temperature)

Because DMSO has a better coordination capacity with PbI2 than the commonly used DMF, it is used in this method. After annealing at 100 LC, the very homogenous and flat precursor film was converted into a pure crystalline CH3NH3PbI3 perovskite layer. As shown in Figs. 1, 2, and 3, and Table 1, CH3NH3PbI3 films grown by dropwise CB had better morphological, crystalline, and photovoltaic properties than perovskite layers grown by TO droplet treatment, as shown in Figs. 1, 2, and 3. During the spin-off stage, a highly volatile solvent like TO might expect a substantial amount of evaporation. The rapid evaporation of the casting TO solvent may alter fluid rheology and vice versa, resulting in rough precursor films. Due to its relatively high boiling point and lower vapour pressure

compared to TO, CB has a reduced evaporation rate, which should help build a flatter, smoother, and more uniform MAI– DMSO-PbI2 intermediate phase layer. After heat treatment at 100 LC, the higher quality intermediate phase layer resulted in a more highly crystalline and homogenous CH3NH3PbI3 perovskite capping layer atop the mp-TiO2, resulting in lower series resistance, higher shunt resistance, and improved solar performance in the PSC Figure-3; Table 1. The PCE of the CB-treated HTM-free PSCs was 9.73 percent, which is 71 and 36 percent higher than the controls generated from pristine perovskite film and TO droplet treatment, respectively. The increased device performance confirmed the importance of CB droplets in HTM-free PSC improvement without a doubt. The HTM-free PSCs form on the inclusion of CB attained a PCE of 11.44 percent after further adjusting the annealing temperature.

Furthermore, the HTM-free solar cells generated are noticeably more stable than the spiro-OMeTAD HTM-form devices with Ag electrode shown in Fig. 8. After 120 days, the PCE of the carbon-form device was over 8%, while the efficiency of the HTM-form cell was barely 3% after 5 days. We anticipate that our findings will aid in the creation of low-cost, stable PSCs by providing a better knowledge of crystalline perovskite film generation in solvent-assisted procedures.

IV. CONCLUSION

The type of DC solvent and annealing temperature used during the solvent-assisted method to make CH3NH3PbI3 films have a significant impact on the absorber morphologies, crystalline structures, and device photovoltaic performance. When comparing the J–V curves and PCEs of carbon-form HTM-free CH3NH3PbI3 prepared devices with CB or TO as a DC solvent to devices prepared without a DC solvent, the benefits of utilising CB as an aid solvent become clear. The CH3NH3PbI3 films developed with CB have better morphological, surface coverage, and crystalline properties than the perovskite layers generated by adding TO the identical conditions during processing. Without the use of DC solvent, the pristine perovskite layers have significantly worse morphological and crystalline properties. The PCEs of devices HTM-free form on CH3NH3PbI3 manufactured with CB are superior. For the CB-assisted procedure, the possessions of the hardening temperature on CH3NH3PbI3 film shape, crystal structure, and solar cell performance were investigated. Using an optimum annealing temperature of 120 LC, high-efficiency carbon-form HTM-free solar cells with a PCE of 11.44 percent were developed. This paper presents a simple, reliable, and low-cost fabrication technique for inorganic–organic hybrid heterojunction solar cells.

REFERENCES

[1] H.J. Snaith. (2014). Efficient hybrid solar cells form on meso-superstructured orga-nometal halide perovskites. Science 338(6107), 643–647.

[2] M.B. Johnston, & H.J. Snaith. (2017). Efficient planar hetero-junction perovskite solar cells by vapour deposition. Nature 501(7467), 395–398.

[3] S.D. Stranks, & R.J. Nicholas. (2018). Carbon nanotube/polymer composites as a highly stable hole collection layer in perovskite solar cells. Nano Lett, 14(10), 5561–5568.

[4] T. Song. (2016). Interface engineering of highly efficient perovskite solar cells. Science 345(6196), 542–546.

[5] D.W. Zhang. (2019). Graphene-form counter electrode for dye-sensitized solar cells. Carbon 49(15), 5382–5388.

[6] J. Wang. (2020). A bi-layer composite film form on TiO2 hollow spheres, P25, and multi-walled carbon nanotubes for efficient photoanode of dye-sensi-tized solar cell. Nano–Micro Lett.

[7] M.K. Nazeeruddin, & M. Gra¨tzel. (2019). Effect of annealing temperature on film morphology of organic–inorganic hybrid pervoskite solid-state solar cells. Adv. Funct. Mater, 24(21), 3250–3258.

[8] R. Kumar. (2018). Planar heterojunction perovskite solar cells with superior reproducibility.

[9] S. Aharon. (2015). Depletion region effect of highly efficient hole conductor free CH3NH3PbI3 per-ovskite solar cells. Phys, Chem, 16(22), 10512–10518.

[10] J. Shiv., & Ravel N. (2018). (Modified two-step deposition method for high-efficiency TiO2/CH3NH3PbI3 heterojunction solar cells. ACS Appl. Mater. Interfaces 6(12), 9711–9718.